Time-dependent generator coordinate method study of fission: Dissipation effects

Jie Zhao (赵杰) ⓞ,[1] Tamara Nikšić,[2] and Dario Vretenar ⓞ[2,3]

[1]*Center for Circuits and Systems, Peng Cheng Laboratory, Shenzhen 518055, China*
[2]*Physics Department, Faculty of Science, University of Zagreb, Bijenička Cesta 32, Zagreb 10000, Croatia*
[3]*State Key Laboratory of Nuclear Physics and Technology, School of Physics, Peking University, Beijing 100871, China*

Starting from a quantum theory of dissipation for nuclear collective motion introduced by Kerman and Koonin [Phys. Scr. **10**, 118 (1974)], the time-dependent generator coordinate method (TDGCM) is extended to allow for dissipation effects in the description of induced fission dynamics. The extension is based on a generalization of the GCM generating functions that includes excited states, and the resulting equation of motion in the collective coordinates and excitation energy. With the assumption of a narrow Hamiltonian kernel, an expansion in a power series in collective momenta leads to a Schrödinger-like equation that explicitly includes a dissipation term, proportional to the momentum of the statistical wave function. An illustrative calculation is performed for induced fission of ^{228}Th. The three-dimensional model space includes the axially symmetric quadrupole and octupole shape variables, and the nuclear temperature. When compared with data for photoinduced fission of ^{228}Th, the calculated fission yields demonstrate the important role of the additional term in the Hamiltonian that explicitly takes into account the dissipation of energy of collective motion into intrinsic degrees of freedom.

I. INTRODUCTION

Among diverse methods that have been developed over many decades to describe the dynamics of low-energy induced fission, the time-dependent generator coordinate method (TDGCM) [1–5] presents the only microscopic approach that can be used to model the entire fission process, from the quasistationary initial state all the way to scission and the emergence of fission fragments. A recent implementation of the TDGCM [6,7], based on the Gaussian overlap approximation, has been successfully employed in a number of fission studies [8–15] that have explored many interesting subjects, such as the influence of static pairing correlations on fission yields, the definition of scission configurations, different approximations for the collective inertia tensor, finite temperature effects, the role of dynamical pairing degrees of freedom, and symmetry restoration.

TDGCM presents a fully quantum-mechanical approach that describes fission dynamics as an adiabatic evolution of collective degrees of freedom. The nuclear wave function is represented by a linear superposition of many-body generator states that are functions of collective coordinates (shape parameters, pairing degrees of freedom). By employing the Gaussian overlap approximation (GOA), the GCM Hill-Wheeler equation of motion for the collective wave function reduces to a local, time-dependent Schrödinger equation in the space of collective coordinates. Given an energy density functional (EDF) or effective interaction, the collective potential and inertia tensor are determined by constrained self-consistent mean-field calculations in the space of collective coordinates. The TDGCM + GOA is particularly suitable for the slow evolution from the quasistationary initial state to the outer fission barrier (saddle point). Beyond the saddle-point fission dynamics becomes dissipative as the nucleus elongates towards scission. The effect of dissipation is to heat the system, modify the path in the multidimensional deformation space, increase the time to scission, and generate fluctuations in various quantities [16]. However, in contrast to models based on time-dependent density-functional theory (TDDFT) [17–25], TDGCM does not contain a one-body dissipation mechanism because it only takes into account collective degrees of freedom in the adiabatic approximation.

Since dissipation of the energy of collective motion into intrinsic degrees of freedom plays an important role in the dynamics of the final stage of the fission process, it is important to extend the adiabatic TDGCM approach to explicitly include nucleon degrees of freedom. This is, of course, very difficult to achieve in a fully microscopic approach. In the Schrödinger collective-intrinsic model (SCIM) [3,26], the coupling between collective and intrinsic excitations is taken into account by a generalization of the GCM based on zero- and two-quasiparticle excitations. Another interesting microscopic approach is the transport theory of Ref. [27], in which the slow evolution of the nuclear shape is treated explicitly, while the fast time-dependent intrinsic excitations (multiquasiparticle states) are described in a statistical approximation. This model is also based on deformation constrained self-consistent mean-field calculations and a generalization of the GCM. The TDGCM extensions of Refs. [3,26,27] both have solid microscopic foundations, but they are also extremely complex, and have yet to be implemented in a realistic calculation of fission dynamics.

In the present study we revive a microscopic theory of dissipation for nuclear collective motion, introduced by Kerman and Koonin in Ref. [28]. Based on a generalization of the GCM generating functions to include excited intrinsic states, and certain statistical assumptions, a quantal equation of motion was derived in both the collective coordinates and excitation energy. With the usual assumption of a narrow Hamiltonian kernel, a Schrödinger-like equation can be derived for the statistical collective wave function, including dissipation. In Ref. [28] the method was illustrated with a simple one-dimensional model calculation of heavy-ion collision. Here we employ this method to extend our implementation of the temperature-dependent TDGCM for induced fission dynamics, to include dissipation effects in the collective space of axial quadrupole and octupole deformations. The formalism is developed in Sec. II. In Sec. III we present an illustrative calculation of charge yields for induced fission of ^{228}Th. Finally, Sec. IV contains a short summary and an outlook for future studies.

II. THEORETICAL FRAMEWORK

The purpose of the present study is to extend the time-dependent generator coordinate method (TDGCM) by including energy dissipation and apply the model to the description of induced fission dynamics. The method is based on the quantum theory of dissipation for nuclear collective motion of Ref. [28].

The derivation starts with a trial TDGCM many-body wave function of the following form:

$$|\Phi(t)\rangle = \sum_n \int d\boldsymbol{q} f_n(\boldsymbol{q}, t)|n\boldsymbol{q}\rangle, \tag{1}$$

where $\boldsymbol{q}$ denotes the set of collective coordinates, n labels the excited states at each value of the collective coordinate $\boldsymbol{q}$, and $f_n(\boldsymbol{q}, t)$ are weight functions. From the time-dependent variational principle

$$\delta \int \langle \Phi(t)|[\hat{H} - i\hbar\partial_t]|\Phi(t)\rangle dt = 0, \tag{2}$$

the matrix integral Hill-Wheeler equation is obtained,

$$\sum_{n'} \int d\boldsymbol{q}'\{\mathcal{H}_{nn'}(\boldsymbol{q}, \boldsymbol{q}')f_{n'}(\boldsymbol{q}', t) \\ -\mathcal{N}_{nn'}(\boldsymbol{q}, \boldsymbol{q}')[i\hbar\partial_t f_{n'}(\boldsymbol{q}', t)]\} = 0, \tag{3}$$

where $\mathcal{H}_{nn'}(\boldsymbol{q}, \boldsymbol{q}') = \langle n\boldsymbol{q}|\hat{H}|n'\boldsymbol{q}'\rangle$ is the Hamiltonian kernel, and $\mathcal{N}_{nn'}(\boldsymbol{q}, \boldsymbol{q}') = \langle n\boldsymbol{q}|n'\boldsymbol{q}'\rangle$ is the norm overlap kernel. It is useful to express Eq. (3) in terms of another set of functions $g_n(\boldsymbol{q}, t)$, defined by

$$g_n(\boldsymbol{q}, t) = \sum_{n'} \int d\boldsymbol{q}' \mathcal{N}_{nn'}^{1/2}(\boldsymbol{q}, \boldsymbol{q}')f_{n'}(\boldsymbol{q}', t). \tag{4}$$

With this transformation, Eq. (3) takes the form

$$i\hbar\partial_t g_n(\boldsymbol{q}, t) = \sum_{n'} \int d\boldsymbol{q}' H_{nn'}(\boldsymbol{q}, \boldsymbol{q}')g_{n'}(\boldsymbol{q}', t), \tag{5}$$

with

$$H_{nn'}(\boldsymbol{q}, \boldsymbol{q}') = \sum_{n_1 n_2} \int d\boldsymbol{q}_1 d\boldsymbol{q}_2 \mathcal{N}_{nn_1}^{-1/2}(\boldsymbol{q}, \boldsymbol{q}_1) \\ \times \mathcal{H}_{n_1 n_2}(\boldsymbol{q}_1, \boldsymbol{q}_2)\mathcal{N}_{n_2 n'}^{-1/2}(\boldsymbol{q}_2, \boldsymbol{q}'). \tag{6}$$

As noted in Ref. [28], the level density for each value of the collective coordinate $\boldsymbol{q}$ is high even at relatively low excitation energies, so that the discrete label n can be separated into a continuous excitation energy variable ϵ, and a degeneracy label λ:

$$\sum_{\lambda, \text{ fixed } \epsilon} = \rho(\boldsymbol{q}, \epsilon)d\epsilon, \tag{7}$$

where $\rho(\boldsymbol{q}, \epsilon)$ denotes the level density at the point $\boldsymbol{q}$ in the collective coordinate space. We can then substitute

$$g_n(\boldsymbol{q}, t) \rightarrow g_\lambda(\boldsymbol{q}, \epsilon; t), \tag{8}$$

$$H_{nn'}(\boldsymbol{q}, \boldsymbol{q}') \rightarrow H_{\lambda\lambda'}(\boldsymbol{q}, \boldsymbol{q}'; \epsilon, \epsilon'), \tag{9}$$

and rewrite Eq. (5) as

$$i\hbar\partial_t g_\lambda(\boldsymbol{q}, \epsilon; t) = \int d\boldsymbol{q}' H_{\lambda\lambda}(\boldsymbol{q}, \boldsymbol{q}'; \epsilon, \epsilon)g_\lambda(\boldsymbol{q}', \epsilon; t) + \sum_{\lambda' \neq \lambda} \\ \times \iint d\boldsymbol{q}' d\epsilon' H_{\lambda\lambda'}(\boldsymbol{q}, \boldsymbol{q}'; \epsilon, \epsilon')g_{\lambda'}(\boldsymbol{q}', \epsilon'; t). \tag{10}$$

Following the prescription of Ref. [28], $g_\lambda(\boldsymbol{q}, \epsilon; t)$ in Eq. (10) is replaced by its average value $\overline{g_\lambda(\boldsymbol{q}, \epsilon; t)}$, and the statistical wave function $\psi(\boldsymbol{q}, \epsilon; t)$ is defined as

$$\overline{g_\lambda(\boldsymbol{q}, \epsilon; t)} = \frac{\psi(\boldsymbol{q}, \epsilon; t)}{\sqrt{\rho(\boldsymbol{q}, \epsilon)}}, \tag{11}$$

where the bar denotes average on λ. Performing the summation of Eq. (10) over λ, one obtains

$$i\hbar\frac{\partial}{\partial t}\psi(\boldsymbol{q}, \epsilon; t) = \int d\boldsymbol{q}' h(\boldsymbol{q}, \boldsymbol{q}'; \epsilon, \epsilon)\psi(\boldsymbol{q}', \epsilon; t) + \sum_{\lambda' \neq \lambda} \\ \times \iint d\boldsymbol{q}' d\epsilon' h(\boldsymbol{q}, \boldsymbol{q}'; \epsilon, \epsilon')\psi(\boldsymbol{q}', \epsilon'; t), \tag{12}$$

with the statistical Hamiltonian kernels are defined as

$$h(\boldsymbol{q}, \boldsymbol{q}'; \epsilon, \epsilon) = \frac{1}{\sqrt{\rho(\boldsymbol{q}, \epsilon)}} \sum_\lambda H_{\lambda\lambda}(\boldsymbol{q}, \boldsymbol{q}'; \epsilon, \epsilon)\frac{1}{\sqrt{\rho(\boldsymbol{q}', \epsilon)}}, \tag{13}$$

$$h(\boldsymbol{q}, \boldsymbol{q}'; \epsilon, \epsilon') = \frac{1}{\sqrt{\rho(\boldsymbol{q}, \epsilon)}} \sum_{\lambda, \lambda' \neq \lambda} H_{\lambda\lambda'}(\boldsymbol{q}, \boldsymbol{q}'; \epsilon, \epsilon')\frac{1}{\sqrt{\rho(\boldsymbol{q}', \epsilon')}}. \tag{14}$$

The usual GCM assumption that the Hamiltonian overlap kernel decreases rapidly with increasing $|\boldsymbol{q} - \boldsymbol{q}'|$ (in comparison to the scale of variations in the statistical wave function ψ), enables an expansion of Eq. (12) in a power series in collective momenta $\boldsymbol{P} = -i\hbar(\partial/\partial\boldsymbol{q})$, leading to a

Schrödinger-like equation

$$i\hbar\partial_t\psi(\boldsymbol{q},\epsilon;t) = \left[h^{(0)}(\boldsymbol{q};\epsilon) - \frac{1}{8\hbar^2}[\boldsymbol{P}^2 h^{(2)}(\boldsymbol{q};\epsilon)] \right.$$
$$\left. - \frac{1}{2\hbar^2}\boldsymbol{P}h^{(2)}(\boldsymbol{q};\epsilon)\boldsymbol{P} \right]\psi(\boldsymbol{q},\epsilon;t)$$
$$+ \frac{i}{2\hbar}\int\{\boldsymbol{P}, h^{(1)}(\boldsymbol{q};\epsilon,\epsilon')\}\psi(\boldsymbol{q},\epsilon';t)d\epsilon', \tag{15}$$

where

$$h^{(n)}(\boldsymbol{q};\epsilon,\epsilon') = \int z^n h(\boldsymbol{q}+z/2, \boldsymbol{q}-z/2;\epsilon,\epsilon')dz, \tag{16}$$

$z = \boldsymbol{q} - \boldsymbol{q}'$, and $h^{(n)}(\boldsymbol{q};\epsilon) \equiv h^{(n)}(\boldsymbol{q};\epsilon,\epsilon)$. The curly brackets in the last term of Eq. (15) denote anticommutation. With the collective potential defined as

$$V(\boldsymbol{q},\epsilon) = h^{(0)}(\boldsymbol{q};\epsilon) - \frac{1}{8\hbar^2}[\boldsymbol{P}^2 h^{(2)}(\boldsymbol{q};\epsilon)], \tag{17}$$

and the collective mass

$$\mathcal{M}(\boldsymbol{q},\epsilon) = -\frac{1}{\hbar^2}h^{(2)}(\boldsymbol{q};\epsilon), \tag{18}$$

Eq. (15) can be written in the final form

$$i\hbar\partial_t\psi(\boldsymbol{q},\epsilon;t) = \left[V(\boldsymbol{q},\epsilon) + \boldsymbol{P}\frac{1}{2\mathcal{M}(\boldsymbol{q},\epsilon)}\boldsymbol{P} \right]\psi(\boldsymbol{q},\epsilon;t)$$
$$+ \frac{i}{2}\int\{\boldsymbol{P}, \eta(\boldsymbol{q};\epsilon,\epsilon')\}\psi(\boldsymbol{q},\epsilon';t)d\epsilon'. \tag{19}$$

The dissipation function $\eta(\boldsymbol{q};\epsilon,\epsilon') = h^{(1)}(\boldsymbol{q};\epsilon,\epsilon')/\hbar$ is anti-Hermitian in the variables ϵ and ϵ', so that the Hamiltonian is still a Hermitian operator. For further details we refer the reader to Ref. [28].

To describe low-energy induced fission dynamics, we employ the framework of finite-temperature TDGCM [11,12]. The extension of TDGCM to include finite-temperature effects presents a first step in going beyond the adiabatic approximation [5], in the sense that excitations of intrinsic degrees of freedom are included through the temperature dependence of the generator states [29,30]. The specific value of the temperature depends on the intrinsic excitation energy of the fissioning nucleus. Because of constant temperature, however, this simple model cannot describe dissipation effects. In the method developed in the present study, the excitation energy ϵ appearing in the Schrödinger-like equation (19) is a function of temperature, and the energy dependent collective potential $V(\boldsymbol{q},\epsilon)$, mass $\mathcal{M}(\boldsymbol{q},\epsilon)$, and dissipation function $\eta(\boldsymbol{q};\epsilon,\epsilon')$ can be expressed in terms of the nuclear temperature T: $V(\boldsymbol{q},T) \equiv V(\boldsymbol{q},\epsilon(T))$, $\mathcal{M}(\boldsymbol{q},T) \equiv \mathcal{M}(\boldsymbol{q},\epsilon(T))$, and $\eta(\boldsymbol{q};T,T') \equiv \eta(\boldsymbol{q};\epsilon(T),\epsilon(T'))$. The generator states in the TDGCM ansatz (1) are determined by thermal occupation probabilities of quasiparticle states ($[1 + e^{\beta E_k}]^{-1}$) at a given temperature (intrinsic energy) and collective coordinate, and the dissipation term in Eq. (19) mixes states corresponding to different temperatures. During the time-evolution of an initial collective state, this term takes into account the temperature increase of the fissioning system. We express Eq. (19) in the

form:

$$i\hbar\partial_t\psi(\boldsymbol{q},T;t) = \left[V(\boldsymbol{q},T) + \boldsymbol{P}\frac{1}{2\mathcal{M}(\boldsymbol{q},T)}\boldsymbol{P} \right]\psi(\boldsymbol{q},T;t)$$
$$+ \frac{i}{2}\int\{\boldsymbol{P}, \mathcal{O}(\boldsymbol{q};T,T')\}\psi(\boldsymbol{q},T';t)dT', \tag{20}$$

with $\mathcal{O}(\boldsymbol{q};T,T') = \eta(\boldsymbol{q};T,T')d\epsilon(T)/dT$.

In the present study we employ the self-consistent multidimensionally constrained (MDC) relativistic Hartree-Bogoliubov (RHB) model [31,32] at finite temperature [11,29,30]. In a grand-canonical ensemble, the expectation value of an operator $\hat{O}$ is given by the ensemble average

$$\langle\hat{O}\rangle = \text{Tr}[\hat{D}\hat{O}], \tag{21}$$

where $\hat{D}$ is the density operator

$$\hat{D} = \frac{1}{Z}e^{-\beta(\hat{H}-\mu\hat{N})}, \tag{22}$$

Z is the partition function, and $\beta = 1/k_B T$ is the inverse temperature with the Boltzmann constant k_B. $\hat{H}$ is the Hamiltonian of the system, μ denotes the chemical potential, and $\hat{N}$ is the particle number operator. The entropy of the nuclear system is $S = -k_B\langle\hat{D}\ln\hat{D}\rangle$. The intrinsic level density ρ is calculated in the saddle-point approximation [33]

$$\rho = \frac{e^S}{(2\pi)^{3/2}D^{1/2}}, \tag{23}$$

where D is the determinant of a 3×3 matrix that contains the second derivatives of the entropy with respect to β and $\nu_\tau = \beta\mu_\tau$ ($\tau \equiv p, n$) at the saddle point.

The finite temperature relativistic Hartree-Bogoliubov (FT-RHB) equations are obtained by minimizing the grand-canonical potential $\Omega = \langle\hat{H}\rangle + TS - \mu_\tau\langle\hat{N}\rangle$. In this work the particle-hole channel is specified by the choice of the relativistic energy density functional DD-PC1 [34], while pairing correlations are taken into account in the Bardeen-Cooper-Schrieffer (BCS) approximation with a finite-range separable pairing force [35]. The parameters of the pairing interaction have been adjusted to reproduce the empirical pairing gaps in the mass region considered in this study [12]. The nuclear shape is parametrized by the deformation parameters

$$\beta_{\lambda\mu} = \frac{4\pi}{3AR^\lambda}\langle Q_{\lambda\mu}\rangle. \tag{24}$$

The shape is assumed to be invariant under the exchange of the x and y axes, and all deformation parameters $\beta_{\lambda\mu}$ with even μ can be included simultaneously. The self-consistent relativistic mean-field (RMF + BCS) equations are solved by an expansion in the axially deformed harmonic-oscillator (ADHO) basis [36]. In the present study calculations have been performed in an ADHO basis truncated to $N_f = 20$ oscillator shells.

The internal excitation energy $\epsilon(T)$ of a nucleus at temperature T is defined as the difference between the total binding energy of the equilibrium RMF + BCS minimum at temperature T and at $T = 0$. The thermodynamical potential relevant for deformation effects is the Helmholtz free

energy $F(T) = E(T) - TS$, evaluated at constant temperature T, where $E(T)$ is the binding energy of the deformed nucleus, and the deformation-dependent energy landscape is obtained in a self-consistent finite-temperature mean-field calculation with constraints on the mass multipole moments $Q_{\lambda\mu} = r^\lambda Y_{\lambda\mu}$.

In the present case the collective coordinates $\boldsymbol{q}$ correspond to the quadrupole $\langle Q_{20} \rangle$ and octupole $\langle Q_{30} \rangle$ mass multipole moments. The collective potential is, therefore, $V(\boldsymbol{q}, T) =$

$\epsilon(T) + F(\boldsymbol{q}, T)$, where $F(\boldsymbol{q}, T)$ is the Helmholtz free energy normalized to the corresponding value at the equilibrium RMF + BCS minimum at temperature T. The mass tensor $\mathcal{M}(\boldsymbol{q}, T)$ is calculated in the finite-temperature perturbative cranking approximation [37,38]

$$\mathcal{M}^{Cp} = \hbar^2 M_{(1)}^{-1} M_{(3)} M_{(1)}^{-1}, \qquad (25)$$

with

$$[M_{(k)}]_{ij,T} = \frac{1}{2} \sum_{\mu \neq \nu} \langle 0|\hat{Q}_i|\mu\nu\rangle \langle \mu\nu|\hat{Q}_j|0\rangle \left\{ \frac{(u_\mu u_\nu - v_\mu v_\nu)^2}{(E_\mu - E_\nu)^k} \left[\tanh\left(\frac{E_\mu}{2k_B T}\right) - \tanh\left(\frac{E_\nu}{2k_B T}\right) \right] \right\}$$
$$+ \frac{1}{2} \sum_{\mu\nu} \langle 0|\hat{Q}_i|\mu\nu\rangle \langle \mu\nu|\hat{Q}_j|0\rangle \left\{ \frac{(u_\mu v_\nu + u_\nu v_\mu)^2}{(E_\mu + E_\nu)^k} \left[\tanh\left(\frac{E_\mu}{2k_B T}\right) + \tanh\left(\frac{E_\nu}{2k_B T}\right) \right] \right\}. \qquad (26)$$

$|\mu\nu\rangle$ are the two-quasiparticle states with the corresponding quasiparticle energies E_μ and E_ν. v_μ^2 are the BCS occupation probabilities, and $u_\mu^2 = 1 - v_\mu^2$.

Equation (20) describes nuclear collective motion with dissipation. In addition to the nondissipative potential and kinetic-energy terms, the dissipative channel coupling is proportional to the momentum of the collective wave function. Even though the dissipation function $\eta(\boldsymbol{q}; \epsilon, \epsilon') = h^{(1)}(\boldsymbol{q}; \epsilon, \epsilon')/\hbar$ could, in principle, be determined in a fully microscopic way, in practice this is extremely difficult. Namely, if one considers even-even nuclei and the collective space consists of purely static deformations, the generator states are time-even, and the time-odd linear term $h^{(1)}(\boldsymbol{q}; \epsilon, \epsilon')$ vanishes because of time-reversal invariance [39,40]. To obtain a nonvanishing contribution on the microscopic level, one would have to consider generator states on a dynamic path that includes the collective momentum conjugate to $\boldsymbol{q}$ (dynamical GCM [39]). However, this doubles the dimension of the collective space and a TDGCM calculation in the space of quadrupole and octupole collective coordinates is no longer feasible. This is why, in an exploratory study, we will approximate the dissipation function with a phenomenological ansatz. As explained in Ref. [28], for complicated nuclear many-body configurations, the sign of the Hamiltonian kernel $h(\boldsymbol{q}, \boldsymbol{q}'; \epsilon, \epsilon')$ changes randomly with variation of the internal excitation energies ϵ and ϵ'. Following the central limit theorem, one would expect that the values of the dissipation function $\eta(\boldsymbol{q}; T, T')$ are random variables whose probability density corresponds to a Gaussian distribution centered around zero. Thus we choose the dissipation function $\eta(\boldsymbol{q}; T, T')$ to be of the form

$$\eta(\boldsymbol{q}; T, T') = \begin{cases} 0, & \beta_2 < \beta_2^0 \\ \eta(T, T'), & \beta_2 \geqslant \beta_2^0 \end{cases} \qquad (27)$$

where the matrix elements $\eta(T, T')$ are Gaussian random variables. β_2^0 is set to 1.5, which is slightly beyond the second fission barrier for the example of fission of ^{228}Th, which will be considered in the next section. The cutoff value β_2^0 is introduced, because for induced nuclear fission one only expects significant dissipation effects in the saddle to scission

phase. Similar to Ref. [28], the root-mean-square value of the Gaussian distribution of the $\eta(T, T')$ random variables reads $\gamma\{\log[\rho(T)]\log[\rho(T')]\}^{1/2}$. In this expression $\rho(T)$ is the intrinsic nuclear level density calculated at the RMF + BCS equilibrium minimum at temperature T, while γ is an adjustable parameter. Note that in Ref. [28] the ansatz $\gamma[\rho(T)\rho(T')]^{1/2}$ was used. However, in the realistic example considered here the level density is much higher, and using the expression without the log functions leads to numerical instabilities. The precise value of γ is not crucial but, of course, its strength must be such to produce a noticeable effect.

To model the dynamics of the fission process we follow the time-evolution of an initial wave packet $\psi(\boldsymbol{q}, T, t = 0)$, built as a Gaussian superposition of quasibound states g_k

$$\psi(\boldsymbol{q}, T, t = 0) = \sum_k e^{(E_k - \bar{E})^2 / (2\sigma^2)} g_k(\boldsymbol{q}, T), \qquad (28)$$

where the value of the parameter σ is set to 0.5 MeV. The collective states $\{g_k(\boldsymbol{q}, T)\}$ and the corresponding energies E_k are solutions of the stationary eigenvalue equation, in which the original collective potential is replaced by a new potential $V'(\boldsymbol{q}, T)$ that is obtained by extrapolating the inner potential barrier with a quadratic form. A more detailed description of this procedure can be found in Ref. [7]. The average energy of the collective initial state is calculated as

$$E_{\text{coll}}^* = \langle \psi(\boldsymbol{q}, T, t = 0)|H_{\text{coll}}|\psi(\boldsymbol{q}, T, t = 0)\rangle, \qquad (29)$$

where $H_{\text{coll}} = V(\boldsymbol{q}, T) + \boldsymbol{P}[2\mathcal{M}(\boldsymbol{q}, T)]^{-1}\boldsymbol{P}$, and the mean energy $\bar{E}$ in Eq. (28) is adjusted iteratively to obtain the chosen value of E_{coll}^*.

The time-evolution is described by Eq. (20), in which the temperature T is treated as the third coordinate. Following the prescription of Refs. [6,7], we have discretized the three-dimensional (3D) space $(\boldsymbol{q}, T)$ with the continuous Galerkin finite-element method. This leads to a large set of coupled, time-dependent Schrödinger-like equations characterized by sparse overlap and Hamiltonian matrices. The solution is evolved in small time steps by applying an explicit and unitary propagator built as a Krylov approximation of the exponential of the Hamiltonian. The time step is $\delta t = 5 \times 10^{-4}$ zs (1 zs

$= 10^{-21}$ s), and the charge and mass distributions are calculated after 4×10^4 time steps, which correspond to 20 zs. As in our recent calculations of Refs. [10–14], the parameters of the additional imaginary absorption potential that takes into account the escape of the collective wave packet in the domain outside the region of calculation [7] are the absorption rate $r = 20 \times 10^{22}$ s^{-1} and the width of the absorption band $w = 1.0$.

The deformation collective space is divided into an inner region with a single nuclear density distribution, and an external region that contains the two separate fission fragments.

The scission hypersurface that divides the inner and external regions is determined by calculating the expectation value of the Gaussian neck operator $\hat{Q}_N = \exp[-(z - z_N)^2 / a_N^2]$, where $a_N = 1$ fm and z_N is the position of the neck [41]. We define the pre-scission domain by $\langle \hat{Q}_N \rangle > 3$ and consider the frontier of this domain as the scission surface. The flux of the probability current through this hypersurface provides a measure of the probability of observing a given pair of fragments at time t [7].

From Eq. (20), the time evolution of the probability density reads

$$\frac{\partial}{\partial t}|\psi(\boldsymbol{q}, T; t)|^2 = -\sum_i \frac{\partial J_i(\boldsymbol{q}, T; t)}{\partial q_i} + \frac{i}{2} \Bigg\{ \psi^*(\boldsymbol{q}, T; t) \int dT' \sum_i \{\partial_{q_i}, \eta_i(\boldsymbol{q}; T, T')\} \psi(\boldsymbol{q}, T'; t) \\ - \psi(\boldsymbol{q}, T; t) \int dT' \sum_i \{\partial_{q_i}, \eta_i(\boldsymbol{q}; T, T')\} \psi^*(\boldsymbol{q}, T'; t) \Bigg\}. \tag{30}$$

The two-dimensional scission hypersurface is embedded in the three-dimensional space $(\boldsymbol{q}, T)$. However, for each value of T we have some value of shape coordinates $\boldsymbol{q}$ which correspond to scission contour (here, $\langle \hat{Q}_N \rangle = 3$) and, thus, by taking these values of the shape coordinates and integrating along T' in the last term of Eq. (30), we would inevitably leave the scission contour. Hence, in calculations of the integrated flux through the scission hypersurface we neglect the last term of Eq. (30), and consider the current

$$J_i(\boldsymbol{q}, T; t) = \hbar \sum_j \mathcal{M}_{ij}^{-1}(\boldsymbol{q}, T) \text{Im} \left(\psi^* \frac{\partial \psi}{\partial q_j} \right), \tag{31}$$

to obtain the usual continuity equation

$$\frac{\partial}{\partial t}|\psi(\boldsymbol{q}, T; t)|^2 = -\sum_i \frac{\partial J_i(\boldsymbol{q}, T; t)}{\partial q_i}. \tag{32}$$

The flux of the probability current $\boldsymbol{J}(\boldsymbol{q}, T; t)$ through the scission hypersurface provides a measure of the probability of observing a given pair of fragments at time t. Each infinitesimal surface element is associated with a given pair of fragments (A_L, A_H), where A_L and A_H denote the lighter and heavier fragments, respectively. The integrated flux $F(\xi; t)$ for a given surface element ξ is defined as [7]

$$F(\xi; t) = \int_{t_0}^t dt' \int_{(\boldsymbol{q}, T) \in \xi} \boldsymbol{J}(\boldsymbol{q}, T; t') \cdot d\boldsymbol{S}, \tag{33}$$

where $\boldsymbol{J}(\boldsymbol{q}, T; t')$ denotes the current Eq. (31). Note that the current $\boldsymbol{J}(\boldsymbol{q}, T; t')$ has only components in the β_2 and β_3 directions. The yield for the fission fragment with mass A is defined by

$$Y(A) \propto \sum_{\xi \in \mathcal{A}} \lim_{t \to \infty} F(\xi; t). \tag{34}$$

The set $\mathcal{A}(\xi)$ contains all elements belonging to the scission hypersurface such that one of the fragments has mass number A.

III. ILLUSTRATIVE CALCULATION: INDUCED FISSION DYNAMICS OF ^{228}Th

As an illustrative example, we have performed a TDGCM calculation of induced fission of ^{228}Th. For this nucleus the charge distribution of fission fragments exhibits a coexistence of symmetric and asymmetric peaks [42]. In the first step, a large-scale MDC-RMF calculation is performed to generate the potential-energy surface, single-nucleon wave functions, and occupation factors in the (β_2, β_3, T) space. The intervals for the collective variables are $-1 \leqslant \beta_2 \leqslant 7$ with a step $\Delta \beta_2 = 0.04$; $0 \leqslant \beta_3 \leqslant 3.5$ with a step $\Delta \beta_3 = 0.05$; and the temperature is varied in the range $0 \leqslant T \leqslant 2.0$ MeV, with a step $\Delta T = 0.1$ MeV.

Figure 1(a) displays the calculated excitation energy of the equilibrium minimum ϵ as a function of temperature T. The excitation energy increases quadratically with temperature, in accordance with the Bethe formula $\epsilon = aT^2$. The intrinsic level density, shown in Fig. 1(b), increases exponentially with the entropy and, therefore, also with excitation energy. The change in slope of the excitation energy and the intrinsic level
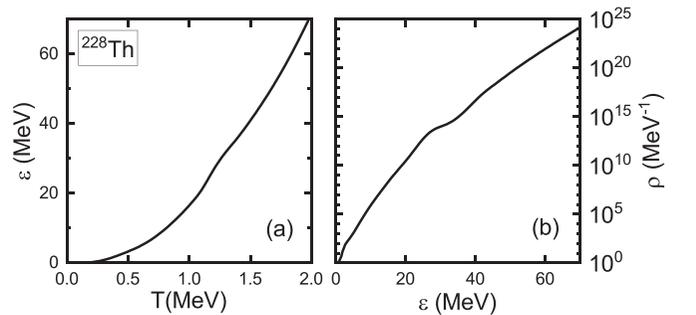
FIG. 1. (a) Excitation energy of the equilibrium (global) minimum ϵ as a function of temperature T, and (b) the intrinsic level density ρ as a function of excitation energy for ^{228}Th, calculated with the finite-temperature RMF + BCS model based on the DD-PC1 functional and finite-range separable pairing.
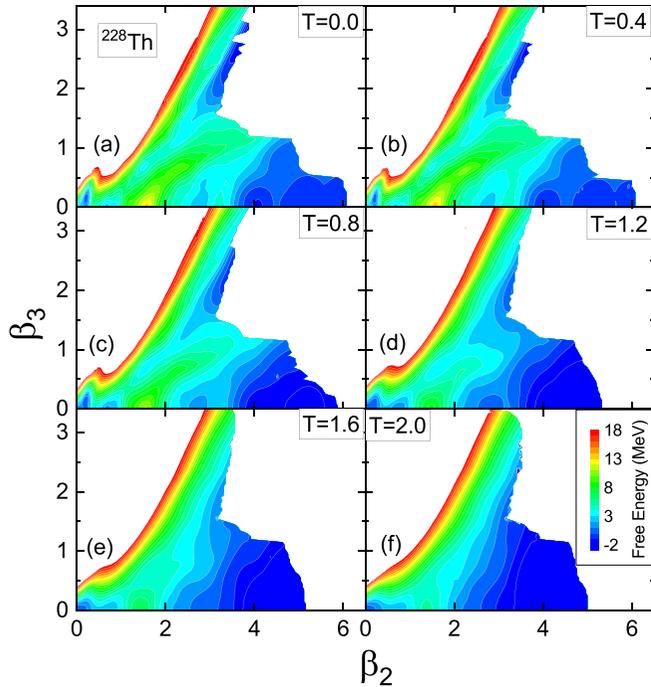
FIG. 2. Free energy manifold of ^{228}Th, calculated with the RMF+BCS model based on the functional DD-PC1 and finite-range separable pairing, projected on the quadrupole-octupole axially symmetric plane, for different values of the temperature T. In each panel energies are normalized with respect to the corresponding value at the equilibrium minimum. Contours join points on the surface with the same energy, and the separation between neighboring contours is 1 MeV.

FIG. 3. Charge yields for induced fission of ^{228}Th at fixed temperatures: $T = 0$, 0.8, 1.0, and 1.2 MeV. The average excitation energy of the initial state E^*_{coll} is chosen 1 MeV above the fission barrier. The data for photoinduced fission correspond to photon energies in the interval 8–14 MeV, and a peak value of $E_\gamma = 11$ MeV [42].

density can be associated with the pairing phase transition at the critical temperature $T_c \approx 0.7$ MeV, and a shape transition at $T \approx 1.2$ MeV. The two-dimensional deformation free-energy surfaces $F(T) = E(T) - TS$, in the collective space (β_2, β_3) for selected values of temperature $T = 0$, 0.4, 0.8, 1.2, 1.6, and 2 MeV, are shown in Fig. 2. Only configurations with $\hat{Q}_N \geqslant 3$ are displayed, and the frontier of this domain corresponds to the scission contour. The deformation surfaces for $T = 0$ and 0.4 MeV are very similar, with a pronounced ridge separating the asymmetric and symmetric fission valleys. For temperatures $T \geqslant 0.8$ MeV this ridge gradually disappears. For $T = 0$ MeV, the scission contour starts from an elongated symmetric point at $\beta_2 \approx 6$, and evolves to a minimal elongation $\beta_2 \approx 3$ as reflection asymmetry increases. For higher temperatures we notice minor qualitative modifications of the scission contour.

To begin with, we have performed a two-dimensional (2D) TDGCM + GOA calculation at fixed temperatures $T = 0$, 0.8, 1.0, and 1.2 MeV (for a detailed description of the model, we refer the reader to Ref. [11]). This calculation does not include dissipation effects. For each temperature, the average excitation energy of the initial state E^*_{coll} is chosen 1 MeV above the fission barrier. The resulting charge yields, normalized to $\sum_A Y(A) = 200$, are displayed in Fig. 3 in comparison to the experimental fragment charge distribution for photoinduced fission of ^{228}Th with photon energies in

the interval 8–14 MeV [42]. The fission yields are obtained by convoluting the raw flux with a Gaussian function of the number of particles, and the width is set to 1.6 units. For $T = 0$ MeV the calculation predicts asymmetric peaks located at $Z = 35$ and $Z = 55$, that is, one charge unit away from the experimental values $Z = 36$ and $Z = 54$. Furthermore, the zero-temperature calculation fails to describe the empirical yields for symmetric fission, and overestimates the asymmetric peaks. Increasing the temperature to $T = 0.8$ MeV brings the theoretical charge yields in fair agreement with the experimental values. For even larger values of temperature $T = 1.0$ MeV and $T = 1.2$ MeV, the description of charge yields deteriorates. In particular, compared with data the symmetric peak is more pronounced, while the asymmetric peaks are underestimated and their position is shifted towards the symmetric peak. This is consistent with the behavior of the free-energy surfaces displayed in Fig. 2, where the ridge between symmetric and asymmetric fission valleys decreases with temperature for $T \geqslant 0.8$ MeV.

In the next step, a full 3D calculation of induced fission dynamics of ^{228}Th is carried out in the space of the axial shape variables (β_2, β_3), and the temperature T. In Fig. 4, the 2D projections on the β_2-β_3 plane of the probability distribution of the initial wave packet are plotted for different temperatures. The average excitation energy of the initial state is $E^*_{coll} = 11$ MeV. In Figs. 5 and 6, we compare the theoretical predictions for the charge yields with the data for photoinduced fission of ^{228}Th [42]. The raw charge yields, normalized to 200, obtained directly from the collective flux through the scission hypersurface are displayed in Fig. 5, while in Fig. 6 we show the convolution of the raw yields with a Gaussian function of width $\sigma = 1.6$ charge units. Results obtained without the inclusion of the dissipation term proportional to
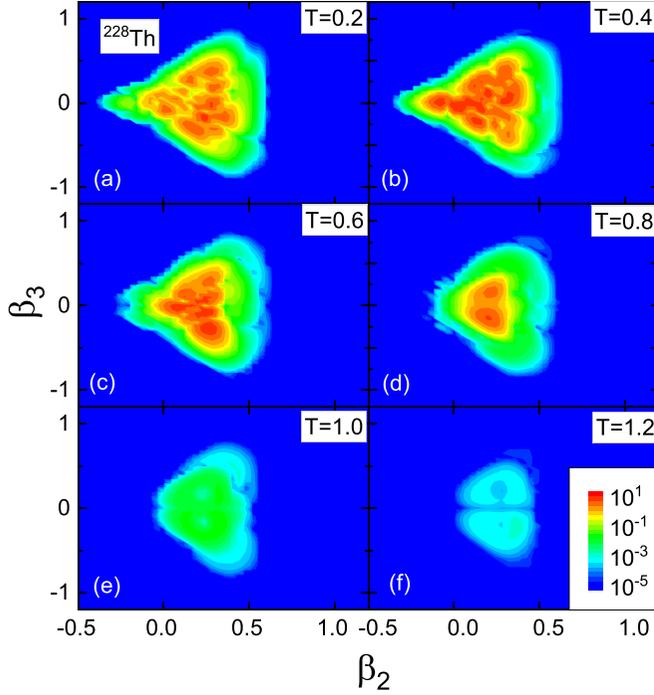
FIG. 4. 2D projections on the (β_2, β_3) plane of the probability distribution of the initial wave packet for induced fission of ^{228}Th, at different temperatures. The average excitation energy of the initial state is $E^*_{\text{coll}} = 11$ MeV.
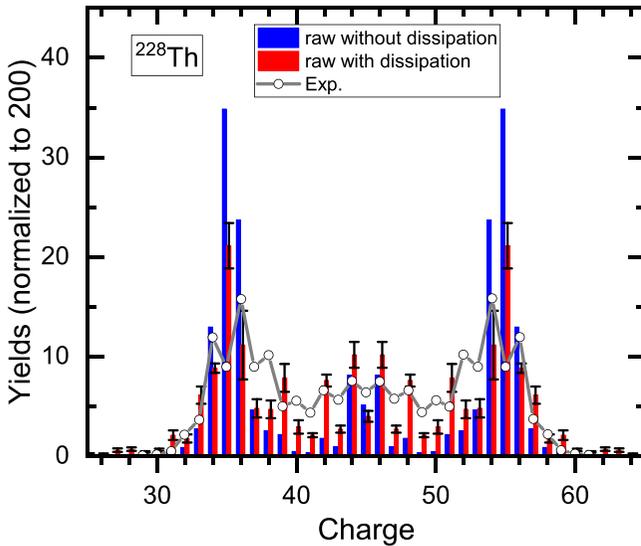
FIG. 5. Raw charge yields (normalized to 200) for induced fission of ^{228}Th, calculated in the 3D space of axial deformation parameters β_2, β_3, and temperature T. The yields obtained without (blue bars) and with (red bars) dissipation are shown in comparison with available data. The results obtained with the inclusion of the dissipation term, correspond to the mean value of five calculations with different random matrices $\eta(T, T')$. The resulting standard deviations are shown as error bars. The data for photoinduced fission correspond to photon energies in the interval 8–14 MeV, and a peak value of $E_\gamma = 11$ MeV [42].
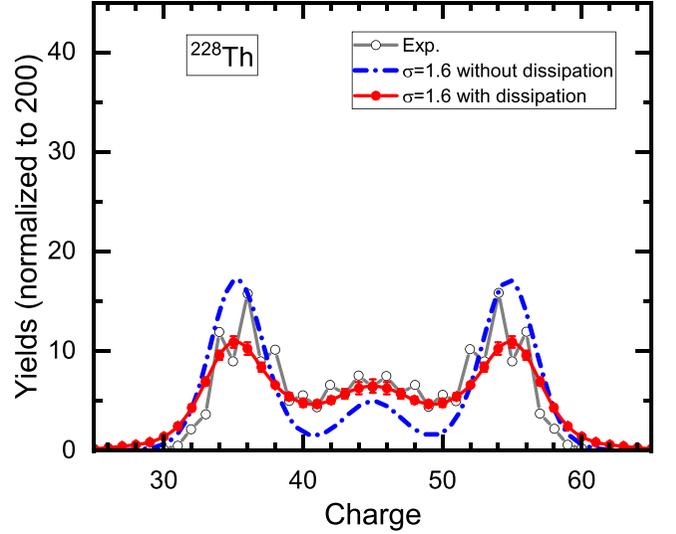
FIG. 6. Same as in the caption to Fig. 5 but for the charge yields obtained by convoluting the raw flux with a Gaussian function of width $\sigma = 1.6$ charge units.

$\eta(q; T, T')$ in Eq. (20) are denoted by blue bars in Fig. 5 and the blue dot-dashed curve in Fig. 6.

When the dissipation term is included in the Hamiltonian of Eq. (20) for the statistical wave function, the results denoted by red bars in Fig. 5, and the red solid curve in Fig. 6 are obtained. Since the matrix elements of the dissipation function $\eta(q; T, T')$ Eq. (27) are assumed to be Gaussian random variables, the calculation has been carried out with five different random matrices $\eta(T, T')$. The results denoted mean values, and the corresponding standard deviations are shown as error bars. Three values of the strength parameter of the dissipation function have been used in the calculation: $\gamma = 0.001$, 0.01, and 0.05. The best agreement with data is obtained for $\gamma = 0.01$. The results displayed in Figs. 5 and 6 demonstrate that, even though the results obtained without dissipation qualitatively reproduce the trend of the data, it is only when dissipation effects are included that experimental charge yields can be reproduced on a quantitative level. We note that a single parameter has been adjusted to experimental results. To illustrate the effect of dissipation on the flux of the probability current through the scission hypersurface, in Fig. 7 we plot the time-integrated flux through the scission contour in the β_2-β_3 plane, for a given value of the temperature T:

$$B(T) \propto \sum_{\xi \in \mathcal{B}} \lim_{t \to \infty} F(\xi; t). \tag{35}$$

The set $\mathcal{B}(\xi \equiv \beta_2, \beta_3)$ contains all elements of the scission contour with a given value T. Without dissipation, a parabolic dependence on temperature is obtained for the time-integrated flux through the scission contour. The parabola, with the maximum at $T \approx 0.3$ MeV, is consistent with the probability distribution of the initial wave packet shown in Fig. 4. When dissipation is included, only the low-T part of the time-integrated flux exhibits a parabolic structure with a maximum at essentially the same temperature. The high-T branch, however, in this case extends to much higher temperatures.
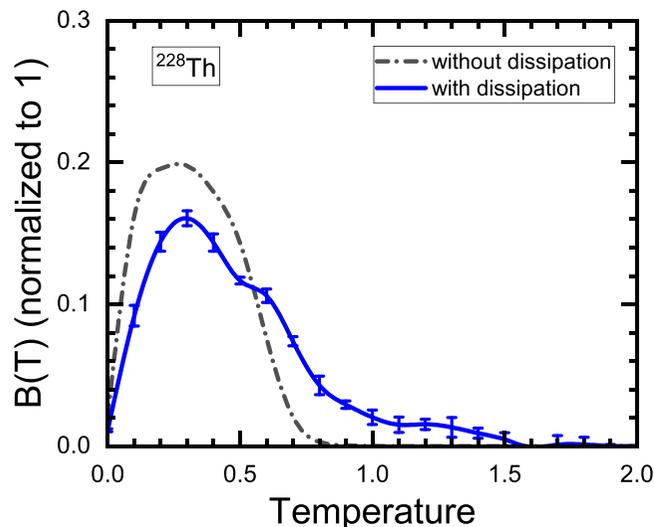
FIG. 7. Time-integrated collective flux $B(T)$ Eq. (35) through the scission contour, as a function of temperature. See caption to Fig. 5 for the explanation of error bars.

While without dissipation no flux through the scission contour is obtained for $T > 0.8$ MeV, dissipation broadens the distribution of the flux and the high-T tail reaches $T \approx 1.5$ MeV. The time-integrated flux nicely illustrates how the inclusion of dissipation in the time-evolution of the collective wave function can describe the heating of the fissioning nucleus in the final saddle to scission phase of fission dynamics.

IV. SUMMARY

Over the last decade various implementations of the time-dependent generator coordinate method (TDGCM) have successfully been applied in the description of the fission process and, in particular, in the calculation of fission yields [3]. However, since TDGCM only includes collective degrees of freedom in the adiabatic approximation, standard formulations of this method cannot take into account the dissipation of the energy of collective motion into intrinsic degrees of freedom. Dissipation heats up the fissioning system, can modify the fission path in the collective space, and affects the time it takes for a nucleus to reach scission [16].

Starting from a quantum theory of dissipation for nuclear collective motion [28], in this work we have extended the temperature-dependent TDGCM for induced fission dynamics, to allow for dissipation effects. The extension is based on a generalization of the GCM generating functions that includes excited intrinsic states. Because the level density is high even at relatively low excitation energies, the discrete label of excited intrinsic states is replaced by a continuous energy variable. By introducing a statistical wave function defined by the average value of the collective wave function and the level density, an equation of motion is derived in the collective coordinates and excitation energy. With the usual assumption that the Hamiltonian overlap kernel decreases rapidly with distance between the corresponding collective coordinates, an expansion in a power series in collective momenta leads to

a Schrödinger-like equation that explicitly includes a dissipation term, proportional to the momentum of the statistical wave function. By expressing the excitation energy in terms of nuclear temperature, the new model can be formulated in the framework of temperature-dependent TDGCM, in which the Helmholtz free energy plays the role of the collective potential, and the collective inertia is calculated in the finite-temperature perturbative cranking approximation.

An illustrative calculation has been performed for induced fission of ^{228}Th, for which the charge distribution of fission fragments exhibits a coexistence of symmetric and asymmetric peaks. The three-dimensional model space includes the axially symmetric quadrupole and octupole shape variables, and the nuclear temperature. The corresponding dissipation function, even though in principle it could be determined microscopically, is approximated by a set of Gaussian random variables, effective in the region of the collective space between the second fission barrier and the scission hypersurface. When compared with data for photoinduced fission of ^{228}Th [42], the calculated fission yields clearly demonstrate the important role of the dissipation term in the Hamiltonian for the statistical wave function. Even though already the finite-temperature TDGCM without dissipation reproduces the empirical trend of the data, it is only with the explicit inclusion of dissipation that theoretical results are obtained in quantitative agreement with the experimental charge yields. As a result of dissipation, a high-temperature tail broadens the distribution of the flux through the scission hypersurface as function of temperature.

The TDGCM extended with the explicit inclusion of dissipation, and the results of the pilot study of induced fission dynamics reported in this work, point to a new microscopic approach that can be employed to quantitatively describe dissipation of the energy of collective motion into intrinsic excitations. Obviously, the next step is to go beyond the statistical ansatz for the dissipation function, and derive it microscopically from the underlying Hamiltonian. An important problem is also the definition of the scission hypersurface in a multidimensional space that includes temperature or intrinsic excitation energy. The interplay between dissipation and pairing degrees of freedom should be explored, as well as the effect of dissipation on the total kinetic-energy distribution.

[1] H. J. Krappe and K. Pomorski, *Theory of Nuclear Fission* (Springer-Verlag, Berlin, Heidelberg, 2012).

[2] N. Schunck and L. M. Robledo, Rep. Prog. Phys. **79**, 116301 (2016).

[3] W. Younes, D. Gogny, and J.-F. Berger, *A Microscopic Theory of Fission Dynamics Based on the Generator Coordinate Method*, Lecture Notes in Physics (Springer, 2019), Vol. 950.

[4] M. Bender *et al.*, J. Phys. G **47**, 113002 (2020).

[5] M. Verriere and D. Regnier, Front. Phys. **8**, 233 (2020).

[6] D. Regnier, M. Verriere, N. Dubray, and N. Schunck, Comput. Phys. Commun. **200**, 350 (2016).

[7] D. Regnier, N. Dubray, M. Verriere, and N. Schunck, Comput. Phys. Commun. **225**, 180 (2018).

[8] D. Regnier, N. Dubray, N. Schunck, and M. Verriere, Phys. Rev. C **93**, 054611 (2016).

[9] D. Regnier, N. Dubray, and N. Schunck, Phys. Rev. C **99**, 024611 (2019).

[10] H. Tao, J. Zhao, Z. P. Li, T. Niksic, and D. Vretenar, Phys. Rev. C **96**, 024319 (2017).

[11] J. Zhao, T. Niksic, D. Vretenar, and S.-G. Zhou, Phys. Rev. C **99**, 014618 (2019).

[12] J. Zhao, J. Xiang, Z.-P. Li, T. Niksic, D. Vretenar, and S.-G. Zhou, Phys. Rev. C **99**, 054613 (2019).

[13] J. Zhao, T. Niksic, D. Vretenar, and S.-G. Zhou, Phys. Rev. C **101**, 064605 (2020).

[14] J. Zhao, T. Niksic, and D. Vretenar, Phys. Rev. C **104**, 044612 (2021).

[15] M. Verriere, N. Schunck, and D. Regnier, Phys. Rev. C **103**, 054602 (2021).

[16] J. R. Nix, Comments Nucl. Part. Phys. **12**, 13 (1983).

[17] C. Simenel, Eur. Phys. J. A **48**, 152 (2012).

[18] C. Simenel and A. S. Umar, Prog. Part. Nucl. Phys. **103**, 19 (2018).

[19] T. Nakatsukasa, K. Matsuyanagi, M. Matsuo, and K. Yabana, Rev. Mod. Phys. **88**, 045004 (2016).

[20] P. D. Stevenson and M. C. Barton, Prog. Part. Nucl. Phys. **104**, 142 (2019).

[21] A. Bulgac, P. Magierski, K. J. Roche, and I. Stetcu, Phys. Rev. Lett. **116**, 122504 (2016).

[22] P. Magierski, K. Sekizawa, and G. Wlazlowski, Phys. Rev. Lett. **119**, 042501 (2017).

[23] G. Scamps and C. Simenel, Nature (London) **564**, 382 (2018).

[24] A. Bulgac, Shi Jin, K. J. Roche, N. Schunck, and I. Stetcu, Phys. Rev. C **100**, 034615 (2019).

[25] A. Bulgac, S. Jin, and I. Stetcu, Front. Phys. **8**, 63 (2020).

[26] R. Bernard, H. Goutte, D. Gogny, and W. Younes, Phys. Rev. C **84**, 044308 (2011).

[27] K. Dietrich, J.-J. Niez, and J.-F. Berger, Nucl. Phys. A **832**, 249 (2010).

[28] A. K. Kerman and S. E. Koonin, Phys. Scr. **10**, 118 (1974).

[29] A. L. Goodman, Nucl. Phys. A **352**, 30 (1981).

[30] J. L. Egido, P. Ring, and H. J. Mang, Nucl. Phys. A **451**, 77 (1986).

[31] B.-N. Lu, J. Zhao, E.-G. Zhao, and S.-G. Zhou, Phys. Rev. C **89**, 014323 (2014).

[32] J. Zhao, B.-N. Lu, E.-G. Zhao, and S.-G. Zhou, Phys. Rev. C **95**, 014320 (2017).

[33] A. Bohr and B. R. Mottelson, *Nuclear Structure*, 1st ed. (Benjamin, New York, 1969), Vol. I.

[34] T. Niksic, D. Vretenar, and P. Ring, Phys. Rev. C **78**, 034318 (2008).

[35] Y. Tian, Z. Y. Ma, and P. Ring, Phys. Lett. B **676**, 44 (2009).

[36] Y. Gambhir, P. Ring, and A. Thimet, Ann. Phys. (NY) **198**, 132 (1990).

[37] Y. Zhu and J. C. Pei, Phys. Rev. C **94**, 024329 (2016).

[38] V. Martin and L. M. Robledo, Int. J. Mod. Phys. E **18**, 861 (2009).

[39] P.-G. Reinhard and K. Goeke, Rep. Prog. Phys. **50**, 1 (1987).

[40] P. Ring and P. Schuck, *The Nuclear Many-Body Problem* (Springer, 1980).

[41] W. Younes and D. Gogny, Phys. Rev. C **80**, 054313 (2009).

[42] K.-H. Schmidt, S. Steinhauser, C. Bockstiegel, A. Grewe, A. Heinz, A. Junghans, J. Benlliure, H.-G. Clerc, M. de Jong, J. Muller, M. Pfutzner, and B. Voss, Nucl. Phys. A **665**, 221 (2000).